J|A|C|S
ARTICLES
Published on Web 05/26/2006

Nuclear and Magnetic Structures and Magnetic Properties of the Layered Cobalt Hydroxysulfate $Co_5(OH)_6(SO_4)_2(H_2O)_4$ and Its Deuterated Analogue, $Co_5(OD)_6(SO_4)_2(D_2O)_4$

Mohsen Ben Salah,[†] Serge Vilminot,*[,†] Gilles André,[‡] Mireille Richard-Plouet,[§] Tahar Mhiri,[#] Seishi Takagi,[||] and Mohamedally Kurmoo*[,⊥]

Contribution from the Groupe des Matériaux Inorganiques, IPCMS, UMR 7504 (CNRS-ULP), 23 rue du Loess, BP 43, 67034 Strasbourg Cedex 2, France, Laboratoire Léon Brillouin, CEA-CNRS, CEA-Saclay, 91191 Gif-sur-Yvette, France, Institut des Matériaux Jean Rouxel, UMR CNRS 6502, Laboratoire de Chimie des Solides, 2 rue de la Houssinière, BP 32229, 44322 Nantes Cedex 03, France, Laboratoire de l'Etat Solide, Faculté des Sciences, Université de Sfax, Route de Sokra Km 4, 3038 Sfax, Tunisia, Department of Physics, Kyushu Institute of Technology, Tobata-ku, Kitakyushu 804-8550, Japan, and Laboratoire de Chimie de Coordination Organique, UMR 7140-CNRS, Université Louis Pasteur, 4 rue Blaise Pascal, 67000 Strasbourg Cedex, France

Received March 6, 2006; E-mail: vilminot@ipcms.u-strasbg.fr; kurmoo@chimie.u-strasbg.fr

Abstract: The structures (nuclear and magnetic), magnetic properties (2−300 K, 1−10^4 bar), and heat capacity of the layered ferromagnet $Co_5(OH)_6(SO_4)_2(H_2O)_4$ are reported. The crystal structure consists of brucite-like M^{II}−OH layers of edge-sharing octahedra, but having two different Co sites, which are pillared by ···O_3SO−$Co(H_2O)_4$−OSO_3···. The absorption spectrum confirms the presence of divalent Co, and by comparison of the two isotopic materials, the assignment of the vibrational spectra is proposed. The magnetic properties are those of a ferromagnet with a Curie temperature of 14 K. Temperature and field dependence magnetization data taken on an aligned sample suggest an easy-plane magnet. The Curie temperature increases linearly with pressure at a rate of +0.12 K/kbar, suggesting small progressive and uniform modifications of the Co−Co exchange interactions. Rietveld refinement of the neutron powder diffraction data and consideration of a group analysis reveal the direction of the moments of the Co within the layer to be along the *b*-axis, with a maximum moment of 3.33 μ_B per cobalt. Those of the pillars remain random. Estimation of the entropy from the heat capacity data accounts for the presence of four ordered moments of Co with spin 1/2 at the long-range ordering temperature, while the moment of the pillaring Co contributes only at lower temperature due to the increase of the internal field as the temperature is lowered. The purely 2D-magnetic ordering in an easy-plane magnet, evidenced by neutron diffraction and heat capacity, challenges the existing theories and is a rare example of a single-layer magnet.

Introduction

Of the many characteristics required in the chemical design of magnetic materials, the most important factor concerns the connections between the moment carriers and the chemical nature of the connectors.[1] From the knowledge acquired, it is clear that there is a logarithmic decrease in the critical temperatures on increasing the number of intervening atoms in the connectors between the metals. Therefore, the Curie temperatures of the transition metals and their complexes tend to decrease in the order metal > metal oxide > metal cyanide > metal bridged by three atom connectors > etc. Among the three-atom connectors, the most naturally abundant are sulfate, phosphate, and carbonate, and these have fascinated magneto-chemists for many years.[1,2] Our on going research is focused on the study of the magnetic properties and the magnetic structures of minerals based on transition metal hydroxysulfates.[3,4] Therefore, we have reproduced the natural conditions in the laboratory using hydrothermal techniques to synthesize several transition metal hydroxysulfates. The advantage over natural minerals is the purity of the materials compared to the multitude of compositions of the natural stones.[5,6] Therefore, interpretations of the magnetic properties are not hampered by

[†] IPCMS, Strasbourg.
[‡] Laboratoire Léon Brillouin.
[§] Institut des Matériaux Jean Rouxel.
[#] Université de Sfax, Tunisia.
[||] Kyushu Institute of Technology.
[⊥] Université Louis Pasteur.

(1) (a) Rado, G. T., Suhl, H., Eds. *Magnetism, A treatise on modern theory and materials*; Academic Press: New York, 1963. (b) Schieber, M. M. *Selected Topics in Solid State Physics, Experimental Magnetochemistry*; Wohlfarth, E. P., Ed.; North-Holland, Amsterdam, 1967; Vol. VIII. (c) Chikazumi, S. *Physics of Ferromagnetism*, 2nd ed.; Clarendon Press: Oxford, 1997. (d) Blundell, S. J. *Magnetism in Condensed Matter*; Oxford University Press, 2001.

(2) (a) Carlin, R. L. *Magneto-Chemistry*; Springer-Verlag: Berlin, 1986. (b) Day, P., Underhill, A. E., Eds. *Metal-Organic and Organic Molecular Magnets, Philos. Trans. R. Soc.*; 1999; Vol. 357. (c) Kahn, O., Ed. *Magnetism: A Supramolecular Function*; Kluwer Academic Publishers: Dordrecht, 1996. (d) Itoh, K., Kinoshita, M., Eds. *Molecular Magnetism, New Magnetic Materials*; Gordon Breach-Kodansha: Tokyo, 2000.

10.1021/ja061302p CCC: $33.50

the presence of other paramagnetic ions. The second advantage is the synthesis of the deuterated analogues for the study of their magnetic structures using neutron diffraction. The additional advantage is that unknown phases are obtained in some cases. This plethora of different phases can at times be frustrating but can also be very informative in deriving structure−property relationships. Our other interest in the use of hydroxide and sulfate as connectors is their modes of coordination, which in many cases produce geometrical frustration[7] and, consequently, unusual magnetic structures, which include the observation of an idle moment, the coexistence of short-range and long-range orderings, continuous temperature dependence of the orientations of moments, and incommensurability.[3] The present paper deals with a ferromagnetic layered cobalt hydroxysulfate having a triangular network.

The study of two-dimensional (2D) quantum spin has been of strong theoretical and experimental interest in recent years.[8] For a purely isotropic 2D layer, such as planar Heisenberg or XY dimensionality,[9] a transition to long-range magnetic order is not theoretically possible at finite temperature,[10] while for an Ising dimensionality such a transition is possible. For the XY system, a vortex structure has been proposed by Kosterlitz and Thouless.[11] The presence of anisotropy, a dipolar field, and/or asymmetric exchange can perturb such a system and introduce some 3D character, which finally results in 3D long-range ordering at finite temperatures.[12] Of particular interest is the orientations of the moments of the carriers and their consequences on the magnetic properties, such as the magnetic hardness. Furthermore, complexities can be envisaged due to geometrical frustration.

Layered compounds can be classified by their structural topologies. There are three main classes. Square or quadratic encompasses the following compounds: $A_2M^{II}X_4$, A = alkali ion or organic ammonium; M = Cu, Cr, Mn; X = halogen.[13] Depending on the metal cation, the ground state can be ferromagnetic or antiferromagnetic. $Ba_2M^{II}(XO_4)$, M = Co, Ni; X = P or As, are examples of hexagonal or honeycomb network.[14] They are antiferromagnets. The triangular lattice can be represented by the following: $M^{II}(OH)_2$ and $M^{II}X_2$, M = Mn, Co, Ni, Fe; X = Cl, Br, I.[15] They crystallize in a $CdCl_2$ structure (or Brucite, $Mg(OH)_2$) where the triangles share edges. They are generally metamagnets arising from weakly antiferromagnetically coupled ferromagnetic layers. Replacing the μ_3-OH by μ_3-O in the $Co(OH)_2$ layers does not alter the layer structure, but the valence state of the cobalt is increased from two to four. Thus doping of the layer by introducing $Na^+(H_2O)_x$ in the galleries creates partial filling of the electronic bands, thus causing the compounds to become semiconducting or metallic and superconducting.[16] The range of values for the band filling results in a very rich physics, especially for the electrical and magnetic properties, for these compounds. Other examples such as $Co_5(OH)_8$(1,4-cyclohexanedicarboxylate)·$4H_2O$, $Co_8(OH)_{12}(SO_4)_2$(diamine)·nH_2O, and $Co_7(OH)_{12}(C_2H_4(SO_3)_2)(H_2O)_2$[17] have periodic vacancies in the brucite layer, and these are capped top and bottom by tetrahedral CoO_4 and all contain ferrimagnetic layers. A special class of triangular lattice is that called Kagomé, where some of the sites in a regular triangular lattice are vacant.[18] The jarosites have such a topology, and they crystallize in the alunite structure where the triangles share vertexes. Although the jarosites are expected not to show long-range magnetic ordering, both ferromagnetism and antiferromagnetism have been evidenced. These examples are all isotropic systems. An example of an anisotropic triangular lattice is shown by $Co_2(OH)_2(C_8H_4O_4)$, consisting of Rutile 110 layers where edge-sharing octahedra chains are orthogonal to one another.[19] It is an unusual metamagnet displaying a rich phase diagram and possibly the hardest molecular magnet known, with a coercive field in excess of 50 kOe at 2 K.

The discovery of the layered material $Co_5(OH)_6(SO_4)_2(H_2O)_4$,[4] having a purely 2D triangular network of spins, was recently reported. The compound showed unexpected ferromagnetic behavior that is substantially different from those previously investigated. It therefore provides an excellent

(3) (a) Vilminot, S.; Richard-Plouet, M.; André, G.; Swierczynski, D.; Bourée-Vigneron, F.; Marino, E.; Guillot, M. *Cryst. Eng.* **2002**, *5*, 177. (b) Vilminot, S.; Richard-Plouet, M.; André, G.; Swierczynski, D.; Guillot, M.; Bourée-Vigneron, F.; Drillon, M. *J. Solid State Chem.* **2003**, *170*, 255. (c) Vilminot, S.; Richard-Plouet, M.; André, G.; Swierczynski, D.; Bourée-Vigneron, F.; Kurmoo, M. *Dalton Trans.* **2006**, 1455. (d) Ben Salah, M.; Vilminot, S.; André, G.; Richard-Plouet, M.; Bourée-Vigneron, F.; Mhiri, T.; Kurmoo, M. *Chem. Eur. J.* **2004**, *10*, 2048. (e) Ben Salah, M.; Vilminot, S.; Mhiri, T.; Kurmoo, M. *Eur. J. Inorg. Chem.* **2004**, 2272. (f) Vilminot, S.; Richard-Plouet, M.; André, G.; Swierczynski, D.; Bourée-Vigneron, F.; Kurmoo, M. *Inorg. Chem*. **2003**, *42*, 6859. (g) Ben Salah, M.; Vilminot, S.; André, G.; Bourée-Vigneron, F.; Richard-Plouet, M.; Mhiri, T.; Kurmoo, M. *Chem. Mater*. **2005**, *17* 2612.

(4) Ben Salah, M.; Vilminot, S.; Richard-Plouet, M.; André, G.; Mhiri, T.; Kurmoo, M. *Chem. Commun.* **2004**, 2548.

(5) See for example: http://webmineral.com/.

(6) (a) Hawthorne, F. C.; Krivovichev, S. V.; Burns, P. C. *Rev. Mineral.* **2000**, *40*, 1. (b) Eby, R. K.; Hawthorne, F. C. *Acta Crystallogr.* **1993**, *B49*, 28.

(7) (a) Bramwell, S. T.; Gingras, M. J. P. *Science* **2001**, *94*, 1495. (b) Greedan, J. E. *J. Mater. Chem.* **2001**, *11*, 37. (c) Ramirez, A. P. In *Handbook of Magnetic Materials*; Buschow, K. J. H., Ed.; Elsevier Science: Amsterdam, 2001; Vol. 13, p 423. (d) Grohol, D.; Matan, K.; Cho, J.-H.; Lee, S.-H.; Lynn, J. W.; Nocera, D. G.; Lee, Y. S. *Nat. Mater.* **2005**, *4*, 323. (e) Diep, H. T., Ed. *Magnetic Systems with Competing Interactions: Frustrated Spin Systems*; World Scientific: Singapore, 1994.

(8) (a) De Jongh, J. J.; Miedema, A. R. *Adv. Phys*. **1974**, *23*, 1. (b) De Jongh, L. J., Ed. *Magnetic Properties of Layered Transition Metal Compounds*; Kluwer Academic Publishers: Dordrecht, 1990.

(9) Mermin, N. D.; Wagner, H. *Phys. Rev. Lett*. **1966**, *17*, 1133.

(10) Onsager, L. *Phys. Rev.* **1944**, *65*, 117.

(11) (a) Kosterlitz, J. M.; Thouless, D. J. In *Progress in Low Temperature Physics*; Brewer, D. F., Ed.; North-Holland: Amsterdam, 1978; Vol. IIB, Chapter 5, p 372. (b) Kosterlitz, J. M.; Thouless, D. J. *J. Phys. C* **1973**, *6*, 1181.

(12) Pokdrovsky, V. L.; Ulmin, G. V. In *Magnetic Properties of Layered Transition Metal Compounds*; De Jongh, L. J., Ed.; Kluwer Academic Publishers: Dordrecht, 1990; p 53.

(13) (a) Bellitto, C.; Day, P. *J. Mater. Chem.* **1992**, *2*, 265. (b) Bramwell, S. T. *J. Phys: Condens. Matter*. **1990**, *2*, 7527. (c) Bloembergen, P. *Physica* **1977**, *85B*, 51. (d) Algra, A. H.; De Jongh, L. J.; Carlin, R. L. *Physica* **1978**, *93B*, 24.

(14) (a) Eymond, S.; Durif, A. *Mater. Res. Bull.* **1969**, *4*, 595. (b) Regnault, L. P.; Rossat-Mignod, J. In *Magnetic Properties of Layered Transition Metal Compounds*; De Jongh, L. J., Ed.; Kluwer Academic Publishers: Dordrecht, 1990; p 271.

(15) (a) Lines, M. E. *Phys. Rev*. **1963**, *131*, 546. (b) Birgeneau, R. J.; Yelon, W. B.; Cohen, E.; Makovsky, J. *Phys. Rev. B* **1972**, *5*, 2607. (c) Yelon, W. B.; Birgeneau, R. J. *Phys. Rev. B* **1972**, *5*, 2615. (d) Wilkinson, M. K.; Cable, J. W.; Wollan, E. O.; Koehler, W. C. *Phys. Rev.* **1959**, *113*, 497. (e) Day, P. *Acc. Chem. Res.* **1988**, *211*, 250. (f) Aruga Katori, H.; Katsumata, K. *Phys. Rev. B* **1996**, *54*, R9620. (g) Takada, T.; Bando, Y.; Kiyama, M.; Mitamoto, K. *J. Phys. Soc. Jpn*. **1966**, *21*, 2745.

(16) (a) Takada, K.; Sakurai, H.; Takayama-Muromachi, E.; Izumi, F.; Dilanian, R.; Sasaki, T. *Nature* **2003**, *422*, 53. (b) Badding, J. V. *Nat. Mater*. **2003**, *2*, 208. (c) Schaak, R. E.; Klimczuk, T.; Foo, F. L.; Cava, R. J. *Nature* **2003**, *424*, 527. (d) Mistry, S.; Arnold, D. C.; Nuttall, C. J.; Lappas, A.; Green. M. A. *Chem. Commun.* **2004**, 2440.

(17) (a) Kurmoo, M.; Kumagai, H.; Hughes, S. M.; Kepert, C. J. *Inorg. Chem.* **2003**, *42*, 6709. (b) Rujiwatra, A.; Kepert, C. J.; Claridge, J. B.; Rosseinsky, M. J.; Kumagai, H.; Kurmoo, M. *J. Am. Chem. Soc.* **2001**, *123*, 10584. (c) Rujiwatra, A.; Kepert, C. J.; Rosseinsky, M. J. *Chem. Commun.* **1999**, 2307. (d) Forster, P. M.; Tafoya, M. M.; Cheetham, A. K. *J. Phys. Chem. Solids* **2004**, *65*, 11.

(18) (a) Nocera, D. G.; Bartlett, B. M.; Grohol, D.; Papoutsakis, D.; Shores, M. P. *Chem. Eur. J.* **2004**, *10*, 3850, and references therein. (b) Wills, A. S. *Phys. Rev. B* **2001**, *63*, 064430. (c) Harrison, A. *J. Phys: Condens. Matter* **2004**, *16*, S553. (d) Shores, M. P.; Nytko, E. A.; Bartlett, B. M.; Nocera, D. G. *J. Am. Chem. Soc.* **2005**, *127*, 13462.

(19) Kurmoo, M.; Kumagai, H.; Green, M. A.; Lovett, B. W.; Blundell, S. J.; Ardavan, A.; Singleton, J. *J. Solid State Chem.* **2001**, *159*, 343.

opportunity to verify certain theoretical hypotheses. The additional anisotropy of the Co^{2+} center enhances the theoretical interest in this compound. Here, we present the optical and thermal characterizations and extensive magnetic properties as well as the magnetic structure. All the results point to the presence of near-neighbor ferromagnetic coupling within the layers, resulting in long-range ordering only within the layer, while the interlayer cobalt atom has a randomly oriented moment.

Experimental Section

Chemicals. All chemicals were obtained from Fluka or Aldrich and used as received. Degassed, distilled water for **1H** and degassed heavy water as received for **1D** were used.

Synthesis of $Co_5(OH)_6(SO_4)_2(H_2O)_4$ (1H). An aqueous solution of cobalt sulfate heptahydrate, $CoSO_4 \cdot 7H_2O$ (2.5 g, 8.9 mM in 15 mL of water), was mixed with an aqueous solution of sodium hydroxide, NaOH (0.06 g, 1.5 mM in 5 mL of water), while stirring. The resulting blue suspension was poured in a Teflon-lined stainless steel bomb of 125 cm^3, sealed, and heated at 165 °C for 24 h. After cooling, the crystals of **1H** were retrieved by filtration and washed thoroughly with water, ethanol, and acetone before drying in air.

Synthesis of $Co_3(OD)_6(SO_4)_2(D_2O)_4$ (1D). For neutron powder diffraction the deuterated compound **1D** was prepared using the same procedure as above upon replacing H_2O by D_2O, to replace as much as possible the H for D in the samples. Deuterium reduces the problem of intense background usually observed for hydrogenated samples due to the high incoherent scattering factor of hydrogen. The crystals of **1D** were found to have over 90% deuterium.

Characterization. Thermal analysis was performed in air by use of a TG-DTA92 Setaram apparatus, at a 6 °C/min heating rate. Infrared spectra were recorded on an ATI Mattson spectrometer by transmission through a KBr pellet containing 1 wt % of the compound. The UV−visible spectrum of **1H** was recorded on a Hitachi U-3000 spectrometer by transmission through an array of crystals held in a PMMA matrix. Powder X-ray diffraction patterns were recorded using a D500 Siemens diffractometer (Co $K\alpha_1$ radiation, $\lambda = 1.789$ Å), equipped with a forward monochromator. The Bragg−Brentano geometry was employed.

The neutron diffraction experiments were performed at the Laboratoire Léon Brillouin (CEA-Saclay) using the G4.1 diffractometer. Data obtained from the multidetector (800 cells) G4.1 ($\lambda = 2.4266$ Å) were used for the determination of the magnetic structure and its thermal evolution at temperatures below 50 K. Therefore, 10 diffraction patterns were recorded in the 2θ range 4−83.9°, at different temperatures between 1.4 and 50 K. The powder sample was held in a cylindrical vanadium container and placed in a liquid helium cryostat. Nuclear and magnetic structures were refined using FULLPROF.[20] The nuclear scattering lengths ($b_{Co} = 0.2490 \times 10^{-12}$ cm, $b_S = 0.2847 \times 10^{-12}$ cm, $b_O = 0.5803 \times 10^{-12}$ cm, $b_D = 0.6671 \times 10^{-12}$ cm, and $b_H = -0.3739 \times 10^{-12}$ cm) and cobalt magnetic form factors were those included in this program.

Magnetization measurements of **1H** and **1D** were performed on several samples from different batches as a polycrystalline sample or an array of oriented crystals for the former. To avoid contamination from other magnetic phases, the crystals were carefully selected under an optical microscope and washed with ethanol prior to the measurements. Data were taken by means of a Quantum Design MPMS-XL SQUID magnetometer. Isothermal magnetization was measured at various temperatures in field spanning ±50 kOe. AC magnetization measurements were performed using the same apparatus in zero dc magnetic field and an alternating field of 1 Oe oscillating at different fixed frequencies from 17 to 1000 Hz. Preparation of the sample consisting of crystals in PMMA is described in ref 17a. A sample for measurement of the pressure dependence was prepared by mixing ca. 20 mg of crystals with Apiezon-J and placed between two layers of NaCl also mixed with Apiezon-M inside a 3 mm diameter Teflon tube. The final sample is therefore a barrel of 3 mm length and 3 mm diameter and has the same size barrels of NaCl on each side. A small ball of high-purity lead of ca. 1 mg was placed in the middle of the sample as a pressure sensor, where the pressure is linearly related to the superconducting transition temperature of lead.

Heat capacity was measured on a homemade pseudoadiabatic apparatus using a ca. 200 mg pellet of the compound wrapped in aluminum. The correction for the aluminum contribution to the heat capacity was made by subtracting its experimentally recorded temperature dependence. The temperature is limited to the range 1.6 to 35 K. Data were recorded reproducibly for two different batches.

Results and Discussion

Synthesis. $Co_5(OH)_6(SO_4)_2(H_2O)_4$ has been reproducibly obtained as pale red plate crystals under certain specific conditions. One is the use of boiled water to eliminate dissolved gases, thus reducing the oxidation of Co^{2+} and the formation of dark oxide phases. The second is to limit the period of the reaction to less than 24 h; otherwise longer periods promote some oxidation. The third is that **1H** is obtained at 165 °C for a NaOH/Co ratio of 0.17, which is far from the expected stoichiometric value of 1.2. Increasing the NaOH/Co ratio and keeping the same temperature promote the formation of $Co_3(OH)_2(SO_4)_2(H_2O)_2$, which appears for a wide range of NaOH/Co ratios.[3g] Increasing the ratio of NaOH/Co to 1.2 and the reaction temperature to 245 °C result in the formation of hexagonal pink plates, which appear to be an anhydrous phase, $Co_5(OH)_6(SO_4)_2$, whose structure remains presently unresolved, and ac and dc magnetic susceptibilities in the range 1.9 to 300 K indicate no long-range magnetic ordering. The fact that the crystals of different phases have different colors and morphologies renders their identification and separation moderately easy.

Powder X-ray Diffraction. The diffraction patterns, obtained using a flat-plate geometry, reveal the presence of a progression of strong Bragg reflections based on 00*l* due to preferential orientations of the plate crystals, the other reflections being weak. For **1H**, the four major reflections are indexed as (00*l*) with $l = 2$, 4, 6, and 8. All the reflections but one at $d = 7.204$ Å, attributed to the strongest line of $Co_3(OH)_2(SO_4)_2(H_2O)_2$, are indexed using the cell parameters deduced from the single-crystal study. For the anhydrous compound, the crystals are much too small for an X-ray measurement and the cell parameters are still unknown. Its powder diffraction pattern reveals a progression of strong, sharp (00*l*) reflections at $d =$ 5.313, 2.65, 1.77, etc., Å and other weak ones at 4.975, 3.54, 2.487, 2.126, and 1.937 Å.[21] These suggest a possible layered structure with an interlayer distance of 5.3 Å, which is half that of the hydrate **1H**.

Infrared Spectroscopy. For the hydrogenated compound **1H**, the infrared spectrum (Figure S1; Table S1) reveals the presence of five families of bands centered around 3400, 1600, 1100, 750, and 600 cm^{-1}. As the bands related to the O−H vibrations are shifted to lower energies upon substitution of H with D, we can, therefore, clearly identify the first, second, and fourth

(20) Rodriguez-Carvajal, J. *FULLPROF: Rietveld, profile matching and integrated intensity refinement of X-ray and/or neutron data*, 3.5d version; Léon-Brillouin Laboratory: CEA Saclay, France, 1998.

(21) Ben Salah, M. Ph.D. Thesis, Université Louis Pasteur, Strasbourg, France, 2004.

families as those related to OH vibrations. Six bands appear between 3600 and 3140 cm^{-1}. According to Nakamoto,[22] these bands can be attributed to OH stretching vibrations. While the first three at 3625, 3607, and 3585 cm^{-1} are very sharp, the remaining ones at 3477, 3354, and 3142 cm^{-1} are broad. From the results of the structure determination, the hydrogen atoms of the OH groups are involved in weak hydrogen bonds with H···O distances higher than 2.25 Å. For the water molecules, the corresponding H···O distances are significantly shorter. Therefore, we propose to attribute the sharp and broad bands to OH and H_2O groups, respectively. This assignment is confirmed by the presence of the higher energy bands and the absence of the lower energy ones for the anhydrous compound, $Co_5(OH)_6(SO_4)_2$. For the deuterated compound (**1D**) (Figure S1), the corresponding family of bands shifts to the range 2680 to 2350 cm^{-1}, i.e., with a ratio ν_{OD}/ν_{OH} close to $(18/17 \times 2)^{1/2}$. At 1630 cm^{-1}, for **1H**, one observes the vibration band related to the deformation of the water molecules. In **1D**, this band is also shifted and appears as a shoulder on the sulfate band centered at 1100 cm^{-1}. The bands at ca. 750 cm^{-1} for **1H** are moved to lower frequencies for the deuterated compound and can be attributed to other OH modes. For the two families of bands showing no deuteration effects, those around 1100 and 600 cm^{-1} are attributed to the ν_3 and ν_4 vibrations of the sulfate group. The sharp band at 972 cm^{-1} has been attributed to the ν_1 mode that becomes IR active with lowering of symmetry of the SO_4 from tetrahedral.

UV−Visible Spectroscopy. The spectrum reveals two broad absorption bands centered at 545 and 497 nm (Figure S2) that are characteristic of cobalt in an octahedral environment. Both bands are responsible for the observed red color of the crystals. They are similar to the ones observed for $Co(H_2O)_6^{2+}$ in solution and correspond to the respective electronic transitions $^4T_{1g}(F) \rightarrow {}^4A_{2g}(P)$ and $^4T_{1g}(F) \rightarrow {}^4T_{1g}(P)$.[23]

Thermal Analysis. The TGA trace (Figure S3) reveals four successive weight losses for **1H** in the temperature range 20 to 1000 °C. The first, between 235 and 270 °C, is related to water loss, and the second from 340 to 420 °C is a combination of the loss of OH as H_2O and the oxidation of Co(II) to Co(III). The sulfate decomposes into SO_3 from 640 to 760 °C, and between 900 and 930 °C Co_3O_4 is reduced to CoO. The final fractional weight of the CoO residue (57.5%) agrees with the value expected (56.7%).

Structure Description of $Co_5(OH)_6(SO_4)_2(H_2O)_4$, 1H. The X-ray single-crystal structure of **1H** (Tables 1, S2, and S3) has been described previously,[4] and therefore, we will keep the discussion brief while highlighting the salient features pertinent to the magnetism presented later. The key feature of the structure is the layer of edge-shared cobalt octahedra (Figure 1) pillared by inorganic ···OSO_3−$Co(H_2O)_4$−O_3SO··· groups. Within the layer the two crystallographically independent cobalt atoms, Co(1) and Co(2), sit on the apexes of an irregular triangular network. They form alternate parallel chains running along the *b*-axis (Figure 2). The connections between the Co atoms are made via the oxygen atoms of the hydroxides and sulfates. The O(2) oxygen atoms of the sulfate group are shared between two

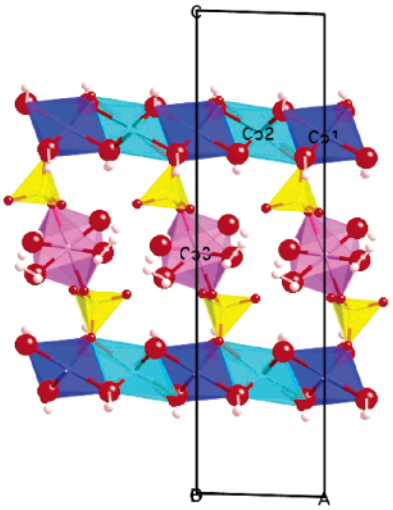

Figure 1. View of the structure of **1H** along the *b*-axis showing the layers pillared by $-OSO_3-Co(H_2O)_4-O_3SO-$.

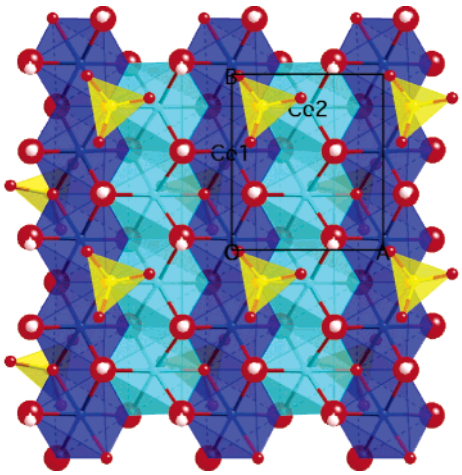

Figure 2. Top view of a single layer of **1H** showing the capping of the sulfate group and the two cobalt chains.

Co(1) and one Co(2), and alternate positions are occupied. On the other face of the layer, the complementary positions are now occupied. The pillaring Co(3) interlayer octahedra connect the sulfate groups. The cobalt octahedra are all distorted to different degrees. That of Co(1) is axially elongated with four short Co−O bonds with hydroxyl groups ($\langle Co-O \rangle = 2.035$Å) and two long ones with O(2) of the sulfate group ($\langle Co-O \rangle =$ 2.264 Å). Co(2) is bonded to five hydroxyl groups ($\langle Co-O \rangle =$ 2.079 Å) and one sulfate O(2) (Co−O = 2.309 Å). The Co(3) octahedron is axially compressed, forming four equidistant bonds with water molecules (Co−O = 2.103 Å) and two with the sulfate O(4) (Co−O = 2.090 Å) in *trans* positions. The sulfate tetrahedron is nearly regular ($\langle S-O \rangle = 1.477$ Å) and contains four different oxygen atoms. It is of μ_4-type, with O(2) bonded to three Co and O(4) to one Co, while O(1) and O(3) are terminal (Figure S4). Concerning the environment of the oxygen atoms, four types are evidenced: μ_1-type for $Co-OH_2$ and S−O; μ_2-type for S−O−Co, μ_3-type for Co_3-OH, and μ_4-type for $S-O-Co_3$. Even if some imprecision remains concerning the hydrogen positions, one observes that all O−H distances are between 0.67 and 0.82 Å, values currently obtained from X-ray analyses. Hydrogen atoms of the hydroxyl groups are involved in weak hydrogen bonds since all H···O distances are

(22) Nakamoto, K. *Infrared and Raman Spectra of Inorganic and Coordination Compounds*; John Wiley: New York, 1986.
(23) (a) Griffith, J. S. *The Theory of Transition Metals Ions*; Cambridge University Press: New York, 1961. (b) Lever, A. P. B. *Inorganic Electronic Spectroscopy*; Elsevier: Amsterdam, 1986.

Table 1. Summary of the X-ray Data (300 K) on a Single Crystal of $Co_5(OH)_6(SO_4)_2(H_2O)_4$ and Neutron Powder Data (18 and 1.4 K) of the Deuterated Analogue

	300 K[a]	18 K	1.4 K
system		monoclinic	
space group		$P2_1/c$	
a (Å)	5.4698(2)	5.4637(6)	5.4700(6)
b (Å)	6.3435(3)	6.3460(5)	6.3530(6)
c (Å)	20.5471(8)	20.475(3)	20.482(3)
β (deg)	91.709(2)	91.681(7)	91.661(7)
V (Å^3)	712.62(5)	709.6(3)	711.5(3)
D_c (g·cm^{-3})	3.080	3.158	3.150
μ (mm^{-1})	6.06		
wavelength (Å)	0.71069	2.4266	
2θ range (step) (deg)	6.7−60.1	4−83.9 (0.1)	
no. of reflns nuclear/magnetic	3593	150/0	150/303
no. of unique reflns	2035		
unique $\lvert F_o\rvert > 4\sigma(F_o)$	1834		
no. of params	144	80	82
R_p (%)		14.7	13.7
R_{wp} (%)		13.6	12.6
R_{exp} (%)	3.79	4.72	4.20
R_B (%)		3.84	3.44
R_F (%)	5.35[b]	3.12	2.32
$wR(F_o^2)$	12.91[b]		
$R_{magnetic}$ (%)			3.44
GoF	1.11		

[a] Reference 4. [b] $R_F = \sum||F_o| - |F_c||/\sum|F_o|$; $wR(F_o^2) = \{\sum[w(F_o^2 - F_c^2)^2]/\sum[w(F_o^2)^2]\}^{1/2}$, $w = 1/[\sigma^2(F_o^2) + (0.0262P)^2 + 1.2P]$ with $P = (\mathrm{Max}(F_o^2,0) + 2F_c^2)/3$.

greater than 2.25 Å. These values are significantly shorter for the hydrogen atoms of water molecules with H···O distances between 1.92 and 2.13 Å, defining slightly stronger hydrogen bonds. Analyses of the neutron diffraction data give more precise positions of the hydrogen atoms and confirm the observations of the X-ray refinements.

The lowering of symmetry of the regular brucite layer from hexagonal to the present monoclinic imposes several distortions within the layer, which is reflected first by the observation of two crystallographically independent cobalt atoms and six different Co−Co distances ranging from 3.107 to 3.219Å. The Co−Co−Co angles of the triangular lattice fall between 58° and 60°. Most importantly for determining the sign and magnitude of the exchange interactions within the layer it is valuable to note the Co−O−Co angles, which lie between 88.8° and 104.3°. These values suggest the presence of both ferromagnetic and antiferromagnetic exchanges (Table 2).[24]

Magnetic Properties at Ambient Pressure. The magnetic properties of **1H** have been studied on polycrystalline samples and on an array of aligned crystals as a function of temperature (2−300 K) and of field (±50 kOe). The magnetic properties of **1D** have been studied only as a function of temperature and shown to be similar to those of **1H**. The temperature dependence of the magnetic susceptibility of **1H** in an applied field of 100 Oe is shown in Figure 3 for the polycrystalline sample and in 1000 Oe for the aligned crystals in PMMA with the field parallel or perpendicular to the layers. The data can be described in two parts, as the compound exhibits long-range ordering at low temperatures (T < 14 K). In the high-temperature region, the susceptibility is described by the Curie−Weiss function, and fit of the inverse susceptibility versus temperature for data above 150 K gives a Curie constant of 14.5(2) emu·K·mol^{-1} and a Weiss temperature of +3 ± 3 K. The Curie constant is for five cobalt atoms, and it translates to 2.9 emu·K·(mol of cobalt)$^{-1}$. From this value, we get an effective moment of 4.82 μ_B. This value is larger than that expected assuming only the spin quantum numbers but is within the range observed for most Co(II) systems. This enhancement is associated with the orbital contribution due to the presence of spin−orbit coupling (S = 3/2 and effective orbital quantum number L = 1). Being a Kramer's ion with a considerable spin−orbit coupling (−180 cm^{-1}), the effective spin is 3/2 at high temperatures and is reduced to 1/2 at low temperatures. For this effective spin reduction, Mabbs and Machin[25] relate it to a virtual Weiss constant of ca. −20 K for noninteracting Co atoms. Taking this as an argument, we can therefore assume that in the title compound the interaction between nearest neighbors within the layer is ferromagnetic. The values for the data obtained for a field parallel and perpendicular to the layers are close to those above. The slight deviations at high temperatures only demonstrate the small anisotropy.

The second region concerns the temperatures below 14 K. In a field of 100 Oe, the magnetization quickly saturates and the saturation values are very different for the two orientations. To understand the magnetic properties in this region, we have measured the magnetization in a small ac or dc field for zero-field-cooling (ZFC) and field-cooling (FC) modes. The results are presented in Figure 4a. Following ZFC, the magnetization was measured on warming in a field of 1 Oe for the polycrystalline sample and 10 Oe for the aligned crystals sample to a temperature above the critical temperature and then on cooling in the same field. The dc data show very weak magnetization on warming, suggesting that **1H** consists of magnetic domains until it reaches a maximum at 13.3 K. It has a bifurcation with the data taken on cooling at 14 K, which defines the Curie temperature of the magnet. On further cooling, the magnetization saturates. The ac susceptibilities (Figure 4b) are characterized by one peak for both the real and imaginary components. The temperature at the peak maximum for the real component does not coincide with the temperature at which the imaginary part becomes nonzero. This may suggest that the compound is behaving more like a 2D than a 3D magnet. The sharp peaks in the ac susceptibilities are consistent with the presence of magnetic hardness. The lack of any shift in temperature at the peak maximum of the real component and at the nonzero value of the imaginary component for the range of frequencies of the oscillating field confirms the absence of any glasslike behavior.[26]

The isothermal magnetization at 2 K was studied for the polycrystalline sample as well as for the oriented crystals sample (Figure 5). The first observation is the presence of a hysteresis loop with a coercive field of 580 Oe for the polycrystalline sample and 650 and 2100 Oe for the aligned crystals for fields parallel and perpendicular to the layers, respectively. The second observation is that the magnetization in 50 kOe has a value of 9.67 μ_B for the polycrystalline sample, which indicates all the moments are almost aligned with the field. A saturation value of 11 μ_B is anticipated if we take into consideration that the cobalt has an effective spin of 1/2 and a very anisotropic g-value

(24) Goodenough, J. B. *Magnetism and the Chemical Bond*; John Wiley and Sons: New York, 1963.

(25) (a) Mabbs, F. E.; Machin, D. J. *Magnetism and Transition Metal Complexes*; Chapman and Hall: London, 1973. (b) Lines, M. E. *J. Chem. Phys.* **1971**, *55*, 2977.

(26) Mydosh, J. A. *Spin Glasses: An Experimental Introduction*; Taylor and Francis: London, 1993.

Table 2. Selected Interatomic Distances (Å) and Angles (deg) from X-ray Structure Determination of **1H**

S−O3	1.463(4)	Co1−OH3	2.028(3)	Co2−OH3	2.044(3)	Co3−O4	2.090(3) × 2
S−O1	1.466(3)	Co1−OH2	2.033(3)	Co2−OH1	2.069(3)	Co3−OW1	2.103(4) × 2
S−O4	1.470(3)	Co1−OH1	2.038(3)	Co2−OH3	2.082(3)	Co3−OW2	2.103(3) × 2
S−O2	1.509(3)	Co1−OH2	2.039(3)	Co2−OH2	2.098(3)	⟨Co3−O⟩	2.099
⟨S−O⟩	1.477	Co1−O2	2.245(3)	Co2−OH1	2.100(3)		
		Co1−O2	2.283(3)	Co2−O2	2.309(3)		
		⟨Co1−O⟩	2.111	⟨Co2−O⟩	2.117		
Co1−Co1	3.172	Co2−Co2	3.176	Co1−Co2	3.108, 3.219, 3.213, 3.107		
Co1−O−Co1	88.9 102.3	Co2−O−Co2	100.7 99.3	Co1−O−Co2	88.8, 89.9, 98.2, 104.2, 103.2, 97.6, 97.4, 97.3		

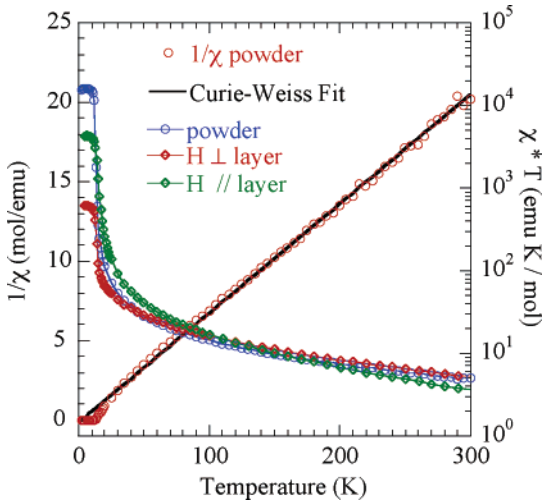

Figure 3. Temperature dependence of χT on a semilog scale for a polycrystalline sample (100 Oe) and for an aligned array of crystals (1000 Oe) with the field applied perpendicular and parallel to the layers. The $1/\chi$ dependence for the polycrystalline sample and a Curie−Weiss fit are also shown.

(13/3 average). The third observation is the anisotropy where the magnetization is larger for a field applied parallel to the layers than when it is perpendicular, suggesting the easy axis lies in the plane. Therefore, we can classify this compound as an easy-plane ferromagnet. The isothermal magnetization (Figure S5) was measured at four temperatures (2, 5, 10, and 12 K) for a field applied parallel to the layer; the coercive field decreases on increasing temperature (being 650, 75, 0, and 0 Oe, respectively). The remanent field (Figure S6) increases on lowering the temperature and the shape becomes square. We have to note that there is a deviation in the field dependence of the magnetization for a field above 20 kOe for the 2 K data compared to those at other temperatures.

An interesting aspect of the hysteresis concerns the rapid rise in magnetization at low field and the slow linear dependence above 2 kOe. One can possibly conclude that the moments within the layer are well ordered due to the short distances between the cobalt atoms and the magnetic superexchange through only the hydroxide. Considering the Co−Co distances and the Co−O−Co angles (Table 2) and using Goodenough−Kanamori[24,27] arguments, we can conclude that these exchange interactions can be both ferromagnetic and antiferromagnetic. However, we cannot estimate their magnitudes without going into lengthy calculations, and this is not the purpose of the present paper. The value of the Weiss temperature suggests that the ferromagnetic exchange interactions dominate.

(27) (a) Kanamori, J. *J. Phys. Chem. Solids* **1959**, *10*, 87. (b) Kanamori, J. In *Magnetism*; Rado, G. T., Suhl, H., Eds.; Academic Press: New York, 1963; Vol. I, Chapter 4, p 127.

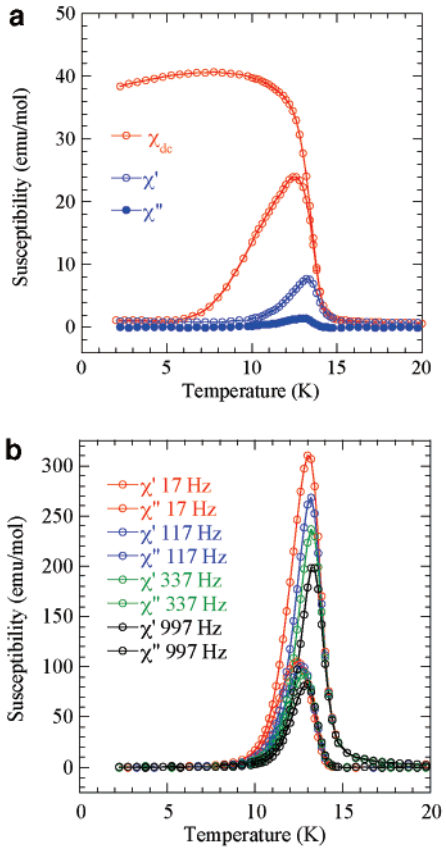

Figure 4. (a) Temperature dependence of the ZFC/FC dc susceptibility (H = 10 Oe) and the ac susceptibilities (H = 1 Oe, 17 Hz) for H parallel to the layers. (b) Temperature dependence of the ac susceptibilities in 1 Oe for different oscillating frequencies from 17 to 997 Hz for H parallel to the layers.

The short Co−Co distances and favorable Co−O−Co angles should enhance the correlation between moment carriers to long distances as the Curie temperature is approached from the high end. It is clear in the small field measurements (Figure 4a) that there is a progressive increase of the correlation that results in the buildup of giant effective moments, and dipolar or weak through-bond interaction between neighboring layers consequently drives the 3D long-range ferromagnetic ordering. It is therefore likely that the interlayer $Co(H_2O)_4$ is not ordered but adds a Brillouin-like isothermal magnetization on increasing the applied field strength, which is a linear dependence at high field. We note that the value of nearly 8 μ_B at the remanence, amounting to only the cobalt moments within the layers, is in good agreement with the above hypothesis. This hypothesis is confirmed by the neutron diffraction study and also by the specific heat data (see later). The temperature dependence of the remanent magnetization is again anisotropic for the two

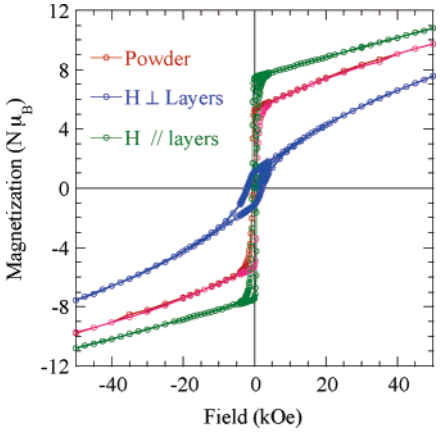

Figure 5. Isothermal magnetization at 2 K for a polycrystalline sample (red) and for an array of aligned crystals with the field parallel (green) and perpendicular (blue) to the layers.

orientations studied. It decreases rapidly on increasing the temperature and becomes zero near the transition temperature. However, the degree of anisotropy eliminates the possibility of an Ising description for this compound.

In the crystal structure, all the layers are identical, although there are two layers per unit cell. Considering only the cobalt and the bridging oxygen atoms within a single layer, we can define six exchange-coupling constants, J_1 (Co1−Co1), J_2 (Co2−Co2), and J_3 to J_6 (Co1−Co2) (Figure S7). The Co−Co distances lie in the range 3.107−3.219 Å and the Co−O−Co angles lie in the range 88.8−104.2°, both favorable for strong coupling. The type of 3D magnetic ordering will depend on the balance between through-space dipolar interaction and exchange through-bonds across the bridging pillar, $O_3SO-Co-OSO_3$. If dipolar is the dominant mechanism, two cases can be defined; one is when the moments are perpendicular to the layer, which is expected to drive the compound to a ferromagnetic ordering, and when it is parallel, to an antiferromagnetic ordering. On the other hand, depending on the sign of the exchange interlayer coupling, either a ferromagnetic or antiferromagnetic ordering is possible. In case of the latter, a magnetic field larger than a critical one that is proportional to the interlayer exchange constant may be able to reverse the direction of the moments. Our case is on a borderline between the exchange and dipolar mechanism and, therefore, is very critical to the applied field. Furthermore, the presence of an extra moment between the layers makes it difficult to propose a ground state.

Magnetic Properties under Applied Pressure. To verify if it is possible to change the magnetic dimensionality of the compound, we have studied the dependence of the magnetization as a function of pressure up to 10 kbar using a SQUID magnetometer and a home-built Cu−Be clamp pressure cell.[28] We have therefore performed field-cooled ac and dc magnetization measurements from 50 to 2 K in a dc field of only 2 Oe and an ac field of 2 Oe oscillating at 37 Hz. We should point out that the eddy current produced by the alternating current field, especially at high field, perturbed the phase shifts and, consequently, results in an overestimated imaginary component of the ac susceptibility at the cost of the real component. However, it does not affect the position of the peak in the ac

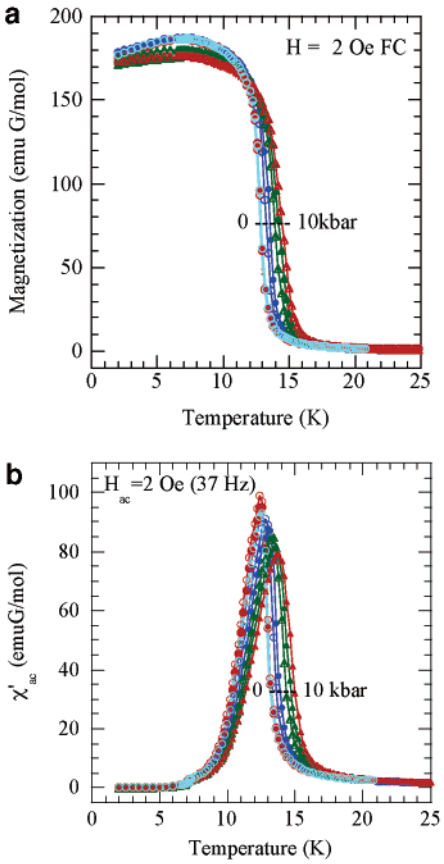

Figure 6. (a) Temperature dependence of the dc magnetization of a polycrystalline sample in an applied field of 2 Oe measured on cooling at different applied pressures. Note that the data at 1 bar are reversible (red dot for the virgin samples and turquoise circles after the pressure experiments). (b) Temperature dependence of the real part of the ac susceptibilities of a polycrystalline sample in an applied field of 2 Oe oscillating at 37 Hz at different applied pressures. Note that the data at 1 bar are reversible (red dot for the virgin sample and turquoise circles after the pressure experiments).

susceptibilities to a great extent. Therefore, the results of only the dc and the real part of the ac susceptibilities are presented in Figure 6. The temperature dependence of the dc magnetization at 1 bar was found to be similar when it was measured in the pressure cell to that in a gelatin capsule or embedded in PMMA. It is also reversible as shown in Figure 6 after depressurizing. On increasing pressure, two effects are observed. The first is the shift of the rapid rise in magnetization, and the second is the disappearance of the broad maximum at 7 K. The rise in magnetization at the Curie temperature is almost the same for all temperatures. The reversibility of the behavior with pressure was verified by measuring the magnetization after depressurizing followed by repressurizing. The ac susceptibility shows similar trends upon applying pressure (Figure 6b). The Curie temperature is better defined by the temperature of the maximum of the real part of the ac susceptibilities. A plot of the Curie temperature as a function of pressure is found to be linear with a slope of 0.123 K/kbar and zero pressure value of 12.6 K (Figure S8). The linear dependence of T_C and the small rate of increase are related to the high density of the compound and the low compressibility. It can also be interpreted as if the pressure affects all the exchange interactions uniformly.

Specific Heat. Specific heat measurements in zero field were performed to investigate the mechanism of the long-range

(28) Mito, M.; Kawae, T.; Takumi, M.; Nagata, K.; Tamura, M.; Kinoshita, M.; Takeda, K. *Phys. Rev. B* **1997**, *56*, 14255.

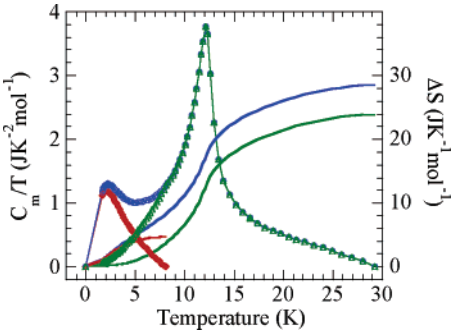

Figure 7. Temperature dependence of magnetic heat capacity normalized to the temperature (experimental data in blue circles, deconvoluted components in red and green circles) and the corresponding integrated entropies in lines.

magnetic ordering of this compound in more detail. Figure 7 shows the experimental temperature dependence of the heat capacity corrected for the lattice phonons as follows:

$$C_m = C_p - C_{lattice}$$

where the lattice contribution is expressed by

$$C_{lattice} = \beta_1 T^3 + \text{higher terms}$$

(higher terms are assumed to be very small in our case and also due to limited temperature range of the measurements) and β_1 is related to the Debye temperature by the following equation:

$$\Theta_D = (234Nk_B/\beta_1)^{1/3} = 105 \text{ K for } \mathbf{1H}$$

The magnetic heat capacity normalized by the temperature shows two anomalies, one at the long-range magnetic ordering discussed above and the other at a much lower temperature of 2.2 K. The former has the characteristic λ-type shape, confirming the long-range magnetic ordering. To understand these two anomalies, we have numerically deconvoluted the peaks in order to estimate the entropy by integrating the C_m/T versus T curve (assuming the heat capacity is zero at 0 K):

$$S_m = \int (C_m/T)\, dT$$

The value of the total entropy up to 30 K is 28.6 J $K^{-1}mol^{-1}$, and those of the individual components are 4.8 and 23.8 J $K^{-1}mol^{-1}$. The total value is close to that expected, $5R \ln(2S + 1)$, for $S = 1/2$. It is also to be noted that the ratio of the two components appoaches 1:4, which will be consistent with the ratio of the number of cobalt per formula unit between the layers to that in the layers. The entropy up to the long-range magnetic ordering at 13 K is about 60% of the total, suggesting that the rest may be due to short-range correlations within the layer. These results suggest full ordering of the moment within the layer, while the one between the layers (Co3) remains random. However, as the temperature is lowered, the moment of Co3 gradually orders. This ordering is most likely due to the combined effect of the internal field and the magneto-crystalline anisotropy field; both increase on lowering the temperature. To verify this hypothesis, we performed a magnetization measurement on cooling a sample in the highest field of our magnet (50 kOe). It is clear from the data (Figure S9) that the first transition at 14 K is broadened due to the near-neighbor ferromagnetic coupling within the layer. Most importantly, there is a further anomaly below ca. 5 K. To highlight this deviation in the magnetization, we fit a polynomial through the data above 7 K and extrapolated it to lower temperatures to show the deviation. We should point out that in such a high field we expect saturation to a constant value of magnetization. Isothermal magnetization at 2 K displays a different curvature at the high-field end compared to those measured at 5, 10, and 12 K (Figure S5). Further discussion will be given in the neutron analysis section. Such an interpretation was also given for Co-formate-dihydrate, which is composed of quadratic layers with Co−O−CH−O−Co connections pillared by O−CH−O−Co-$(H_2O)_4$−O−CH−O bridges and $Mn(acetate)_2(H_2O)_4$.[29]

Magnetic Structure of 1D. Before proceeding to the determination of the magnetic structure from the neutron powder diffraction data, we first refined the nuclear structure on the set of data collected in the paramagnetic region at 18 K. The presence of additional Bragg reflections led us to consider the presence of a second phase, not detected in the batch on which the X-ray powder diffraction was performed. Its diffraction lines were indexed using the TREOR program: $a = 10.8973(9)$ Å, $b = 6.4775(6)$ Å, $c = 10.6420(5)$ Å, $\beta = 108.076°(4)$, monoclinic $P2/m$.[30] Including the contribution of the second phase, the refinement of the nuclear cell of **1D** converged to R-values around 3.5%. A good agreement with the parameters obtained by X-ray single-crystal determination of **1H** is obtained (Table 1). However, the standard deviations are higher. Concerning the H/D atoms, the positions deduced from X-rays are confirmed (Table S4) and the D content estimated from the scattering factors is quite high, around 0.91. The details of data collection and refinement are given in Table 1, the final atomic positions at 18 K in Table S2, and the observed and calculated profiles in Figure S10.

The comparison of the diffraction patterns recorded at 1.4 and 18 K (Figures 8 and S10), i.e., below and above the 3D magnetic ordering temperature, reveals a strong increase of the intensity of the (002) line at $2\theta = 13.65°$. The other differences in intensities are mainly concerned with (00l) and (h00) lines but with much lower differences for the latter. One also observes an increase in intensity of the line at $2\theta = 22.20°$ attributed to the second phase. The absence of additional reflections suggests that the second phase is also a ferromagnet. Moreover, the fact that the (00l) lines are enhanced indicates that the magnetic moments are not aligned along the c-axis.

The temperature dependence of the magnetic structure has been studied for eight temperatures ranging between 1.4 and 15 K. We determined the associated magnetic structure with the help of Bertaut's representation analysis method,[31] applied to the $P2_1/c$ space group with propagation vector $k = (0\ 0\ 0)$ and Wyckoff positions (4e) for Co(1) and Co(2) and (2a) for Co(3). Four one-dimensional irreducible representations are evidenced,[32] Γ_1 to Γ_4, which are associated with basis vectors (magnetic structures) for the cobalt ions in general positions. For Co(3) in special position, the irreducible representations are restricted to two, Γ_1 and Γ_3. Each Γ_i ($i = 1-4$) is implied

(29) (a) Matsuura, M.; Blöte, H. W. J.; Huiskamp, W. J. *Physica* **1970**, *50*, 444. (b) Takeda, K.; Haseda, T.; Matsuura, M. *Physica* **1971**, *52*, 225. (c) Schelleng, J. H.; Raquet, C. A.; Freidberg, S. A. *Phys. Rev.* **1968**, *176*, 708.
(30) Werner, P. E.; Eriksson, L.; Westdahl, M., *J. Appl. Crystallogr.* **1985**, *18*, 367.
(31) Bertaut, E. F. *Acta Crystallogr. A* **1968**, *24*, 217.

Table 3. Components of the Magnetic Moments for the Two Possible Ferromagnetic Structures

	M//*a*	*M*//*b*	*M*//*c*
Γ_1 Co(1) and Co(2)	+ + − −	+ + + +	+ + − −
Γ_1 Co(3)	+ −	+ +	+ −
Γ_3 Co(1) and Co(2)	+ + + +	+ + − −	+ + + +
Γ_3 Co(3)	+ +	+ −	+ +

in Co "magnetic arrangements", according to

$$\text{Co(1) and Co(2) (4e)} \qquad \Gamma_1 + \Gamma_2 + \Gamma_3 + \Gamma_4$$

$$\text{Co(3) (2a)} \qquad \Gamma_1 + \Gamma_3$$

Among the four models only two, namely, Γ_1 and Γ_3, can describe a ferromagnetic structure. For the first one, only the M_y components are nonzero and are all parallel, while for the second one the moments are parallel but in the *xz*-plane, as shown in Table 3, where the sequence "+ + − −" for instance holds for the components of the magnetic moments of the atoms along the crystallographic *a*-axis according to the successive atomic positions as (x, y, z), $(-x, -y, -z)$, $(-x, 1/2+y, 1/2-z)$, $(x, 1/2-y, 1/2+z)$.

The further refinements reveal that two models are possible for the magnetic moments, either Γ_1 with the moments along the *b*-axis or Γ_3 with the moments along the *a*-axis. This result agrees with the fact that the (002) magnetic reflection is the most intense, excluding the orientation of the magnetic moments along the *c*-axis. Consideration of the nuclear structure reveals that Co(1) and Co(2) belong to different chains within the layers. In a first step, both models have been tested with independent magnetic moments for Co(1) and Co(2), but the refinement rapidly diverged. Therefore, refinement has been performed limiting the magnetic moments for Co(1) and Co(2) to be equal. Both models with moment vectors along the *b*-axis (Γ_1) or along the *a*-axis (Γ_3) yield similar results as far as the magnetic factors of merit are concerned, 3.73% and 4.18%, respectively. However, the presence of some intensities due to magnetic components on the (100) and (200) Bragg peaks favors an alignment of the moments along the *b*-axis (Figure 9). The cobalt and nickel dihalides and the vanadium(III) jarosite are also shown to have easy-plane ferromagnetic layers, where weak antiferromagnetic exchange between adjacent layers results in an overall antiferromagnetic 3D ordering.[15a,33] In contrast, the local anisotropy in the iron dihalides forces the moments to be perpendicular to the layers.[15b] The resulting magnetic moment along the *b*-axis has a value of 3.33(3) μ_B. It is slightly higher than 3 μ_B expected for Co(II). It has been explained by a contribution of orbital coupling.[34] Concerning the Co(3) atom, its magnetic component of 0.184(368) μ_B is very small and always less than the standard deviation and therefore was set to zero in the final refinements. Refinement of the data collected between 3 and 11 K shows that the same magnetic structure is

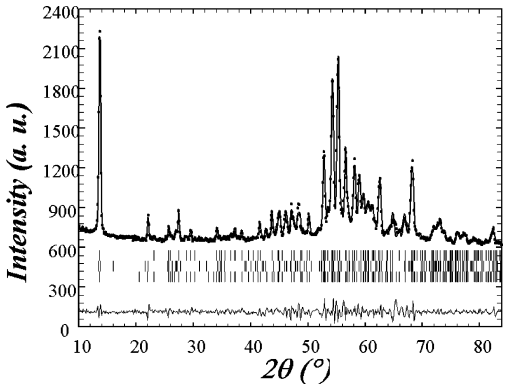

Figure 8. Observed (circles) and calculated (line) profiles of the neutron powder pattern of $Co_5(OD)_6(SO_4)_2(D_2O)_4$ obtained on the G4.1 diffractometer at 1.4 K with position of the Bragg reflections (short vertical lines, nuclear $Co_5(OD)_6(SO_4)_2(D_2O)_4$, impurity, magnetic $Co_5(OD)_6(SO_4)_2(D_2O)_4$) and difference between observed and calculated profiles.

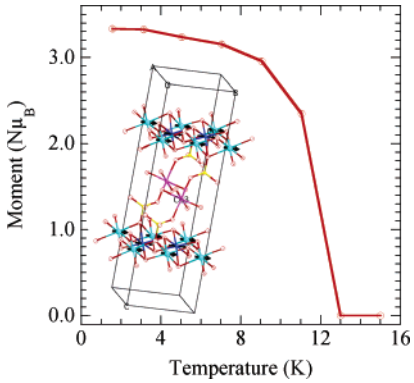

Figure 9. Temperature dependence of the moment of cobalt atoms within the layer. Inset: Magnetic structure of **1D** showing the moments in the layers aligned along the *b*-axis.

observed for all temperatures below T_C. The corresponding temperature dependence of the M_y component of the Co(1) and Co(2) atoms is reported in Figure 9 and shows that the magnetic component is found to be almost constant up to 9 K and slightly decreases at 11 K. However, at the latter temperature, its value is still high, 2.35(4) μ_B.

The observation of only alignment of the moments within the layers in the neutron diffraction and separate peaks for the different cobalt atoms in the heat capacity measurements clearly indicate a novel behavior that can be classified as single-layer magnet (SLM). At present, we have used neutron diffraction and heat capacity measurements to arrive at this conclusion, which was fortuitous by the presence of a paramagnetic ion in the gallery. However, it will be important to develop experiments and theories to fully characterize other materials that may be potential SLM.[35,36]

Conclusion

$Co_5(OH)_6(SO_4)_2(H_2O)_4$ is the first known example of its kind to contain nondefected brucite layers pillared by a paramagnetic entity. The structure provides strong magnetic exchange via Co−O−Co pathways on a triangular lattice and weak Co−O−S−O−Co interlayer exchange through the pillar. Due to the

(32) KAREP, a program for calculating irreducible space group representations: Hovestreydt, E.; Aroyo, I.; Sattler, S.; Wondratschek, H. *J. Appl. Crystallogr.* **1992**, *25*, 544. (b) BASIREPS, a program for calculating nonnormalized basis functions of the irreducible representations of the little group Gk for atom properties in a crystal: Rodriguez-Carvajal, J. Laboratoire Léon Brillouin (CEA-CNRS): CEA Saclay, Gif sur Yvette, France.
(33) (a) Grohol, D.; Huang, Q.; Toby, B. H.; Lynn, J. W.; Lee, Y. S.; Nocera, D. G. *Phys. Rev B* **2003**, *68*, 0944404. (b) Papoutsakis, D.; Grohol, D.; Nocera, D. G. *J. Am. Chem. Soc.* **2002**, *124*, 2647.
(34) Silvera, I. F.; Thornley, J. H. M.; Tinkman, M. *Phys. Rev.* **1964**, *136*, 695.
(35) (a) Talham D. R. *Chem. Rev.* **2004**, *104*, 5479, and references therein. (b) Culp, J. T.; Park, J.-H.; Meisel, M. W.; Talham, D. R. *Inorg. Chem.* **2003**, *42*, 2842.
(36) Heinrich, B., Bland, J. A. C., Eds. *Ultrathin Magnetic Structures*; Springer-Verlag: Berlin, 1994.

structural and single-ion anisotropies, in the magnetically ordered state the moments were found to lie in the plane as found for $Co(OH)_2$. While the magnetic properties are consistent with a weakly anisotropic ferromagnet with a Curie temperature of 14 K, the neutron diffraction and specific heat data suggest long-range ordering of only the moments within the layer, and the one between the layer remains random. At temperatures well below T_C the increasing internal field forces the moment of the interlayer cobalt to align. Although evidence of a dipolar field or an exchange interaction between layers has not been confirmed, their presence cannot be ignored. The magnetic properties of this compound challenge the existing theories and leave the mechanism of ordering of layers an open question. The design of similar compounds will provide test beds for understanding the chemistry and physics of layered materials and thin films of molecular magnetic materials as well as leading the way to single-layer magnets.[35,36]

Acknowledgment. This work was supported by the "Centre National de la Recherche Scientifique", France.

Supporting Information Available: Details of single-crystal X-ray and powder neutron data collection and analysis, and tables of bond distances and angles. Powder neutron diffraction pattern (calculated and experimental). Infrared (including list of bands and assignments) and UV−vis spectra and TGA. Field, temperature, and pressure dependences of the magnetization. This material is available free of charge via the Internet at http://pubs.acs.org.

JA061302P